Biochimie 121 (2016) 179–188

Contents lists available at ScienceDirect

Biochimie

journal homepage: www.elsevier.com/locate/biochi

Research paper

A novel synthetic quinolinone inhibitor presents proteolytic and hemorrhagic inhibitory activities against snake venom metalloproteases

Patrícia T. Baraldi [a, 1], Angelo J. Magro [b, c, d, **, 1], Fábio F. Matioli [d], Silvana Marcussi [e], Ney Lemke [d], Leonardo A. Calderon [f, g], Rodrigo G. Stábeli [f, g], Andreimar M. Soares [f, g], Arlene G. Correa [a], Marcos R.M. Fontes [c, d, *]

[a] Departamento de Química, Universidade Federal de São Carlos (UFSCar), São Carlos, SP, Brazil
[b] Departamento de Bioprocessos e Biotecnologia, Faculdade de Ciências Agrárias, Universidade Estadual Paulista (UNESP), Botucatu, SP, Brazil
[c] Instituto de Biotecnologia, Universidade Estadual Paulista (UNESP), Botucatu, SP, Brazil
[d] Departamento de Física e Biofísica, Instituto de Biociências, Universidade Estadual Paulista (UNESP), Botucatu, SP, Brazil
[e] Departamento de Química, Universidade Federal de Lavras (UFLA), Lavras, MG, Brazil
[f] Centro de Estudos de Biomoléculas Aplicadas à Saúde (CEBio), Fundação Oswaldo Cruz (FIOCRUZ), unidade Fiocruz Rondônia, Porto Velho, RO, Brazil
[g] Departamento de Medicina, Universidade Federal de Rondônia (UNIR), Porto Velho, RO, Brazil

ARTICLE INFO

Article history:
Received 13 August 2015
Accepted 24 November 2015
Available online 14 December 2015

Keywords:
Antihemorrhagic effects
Snake venom
Antiophidic drugs
Quinolinones
Metalloproteases
Bioinformatics studies

ABSTRACT

Metalloproteases play a fundamental role in snake venom envenomation inducing hemorrhagic, fibrige-n(ogen)olytic and myotoxic effects in their victims. Several snake venoms, such as those from the *Bothrops* genus, present important local effects which are not efficiently neutralized by conventional serum therapy. Consequently, these accidents may result in permanent sequelae and disability, creating economic and social problems, especially in developing countries, leading the attention of the World Health Organization that considered ophidic envenomations a neglected tropical disease. Aiming to produce an efficient inhibitor against bothropic venoms, we synthesized different molecules classified as quinolinones – a group of low-toxic chemical compounds widely used as antibacterial and antimycobacterial drugs – and tested their inhibitory properties against hemorrhage caused by bothropic venoms. The results from this initial screening indicated the molecule 2-hydroxymethyl-6-methoxy-1,4-dihydro-4-quinolinone (Q8) was the most effective antihemorrhagic compound among all of the assayed synthetic quinolinones. Other in vitro and *in vivo* experiments showed this novel compound was able to inhibit significantly the hemorrhagic and/or proteolytic activities of bothropic crude venoms and isolated snake venom metalloproteases (SVMPs) even at lower concentrations. Docking and molecular dynamic simulations were also performed to get insights into the structural basis of Q8 inhibitory mechanism against proteolytic and hemorrhagic SVMPs. These structural studies demonstrated that Q8 may form a stable complex with SVMPs, impairing the access of substrates to the active sites of these toxins. Therefore, both experimental and structural data indicate that Q8 compound is an interesting candidate for antiophidic therapy, particularly for the treatment of the hemorrhagic and necrotic effects induced by bothropic venoms.

1. Introduction

Snake venoms are complex mixtures of several proteins including phospholipases A_2, phospholipases A_2-like, metalloproteases, serineproteases, L-amino oxidases, disintegrins, C- type lectins and others. Their combination are able to unleash a complex series of events responsible for the pathophysiology of snake envenomation and the consequent emergence of deleterious

* Corresponding author. Departamento de Física e Biofísica, Instituto de Biociências de Botucatu, UNESP – Campus de Botucatu, Distrito de Rubião Júnior, S/N, CEP:18618-970, Botucatu, SP, Brazil.
** Corresponding author. Departamento de Bioprocessos e Biotecnologia, Faculdade de Ciências Agronômicas (FCA), UNESP – Campus de Botucatu, Fazenda Experimental Lageado, Rua José Barbosa de Barros, 1780, CEP:18.610-307, Botucatu, SP, Brazil.
E-mail addresses: magro@fca.unesp.br (A.J. Magro), fontes@ibb.unesp.br (M.R.M. Fontes).
[1] These authors contributed equally to the work.

http://dx.doi.org/10.1016/j.biochi.2015.11.031
0300-9084/

pharmacological/biological effects like neurotoxicity, myotoxicity, edema-inducing activity, hemorrhage, coagulation and several other properties [1–5].

Recent proteomic analyses indicated that snake venom metalloproteases (SVMPs), which are composed by a group of zinc-dependent enzymes, are the most representative toxins present in viperid species [1–9] and also are found in Colubridae [10–12]; Elapidae [13–16] and Atractaspididae [17] families. According to the revised classification of SVMPs by Fox and Serrano [18,19], these molecules are distributed in three different classes, depending on their molecular weight and domain structure. i) small SVMPs (20–30 kDa) with only a single catalytic domain in the P-I class; ii) medium SVMPs (30–60 kDa) composed by catalytic and disintegrin-like domains in the P-II class; and iii) large SVMPs (60–100 kDa) with catalytic, disintegrin-like and cysteine-rich domains in the P-III class (the large SVMPs with an extra lectin-like domain are also included in the P-III class).

Initially, the main role attributed to SVMPs was related to the remarkable hemorrhagic activity presented by many of these molecules (particularly the large SVMPs). This biological property is clearly linked to their ability to interact with specific receptors on endothelial cells [20,21] and fibroblasts [22] and is also involved in the degradation of extracellular matrix components [23]. However, a wide spectrum of other SVMP functions have been described in the last years, comprising very distinct capabilities as fibrin(ogen) olytic activity, inactivation of blood serine proteinase inhibitors, prothrombin and blood coagulation factor X activation, platelet aggregation inhibition, apoptosis induction, and pro-inflammatory action [24]. All of these activities presented by SVMPs contribute to the systemic actions observed after envenomation, but the influence of these toxins on the local effects is especially critical, since they contribute strongly to severe tissue necrosis resulting from their hemorrhagic and proteolytic activities [25]. Hence, as serum therapy is not effective enough to avoid the occurrence of local effects caused by viperid venoms, it is quite interesting to search for new molecules which could be also used in anti-snake venom treatments.

In many countries, including Brazil, plant extracts are traditionally used for the treatment of snakebite envenomations, although there is scientific validation only in a few cases [26–30]. On the other hand, several isolated plant alkaloids have been described as in vitro and *in vivo* anti-snake venom inhibitors [30–35]. Thus, we synthesized different quinolinone molecules – low-toxic chemical compounds [36] which are already widely used as antibacterial and antimycobacterial drugs [37,38] – and tested their inhibitory properties against hemorrhage caused by *Bothrops jararacussu*, *Bothrops moojeni* and *Bothrops alternatus* venoms and the isolated P-III class SVMP BjussuMP-I from *B. jararacussu*. The results obtained from this initial screening pointed out the most effective antihemorrhagic molecule was the compound 2-hydroxymethyl-6-methoxy-1,4-dihydro-4-quinolinone (identified herein as Q8). Subsequently, other in vitro and *in vivo* experiments showed the novel Q8 compound was able to significantly inhibit, even at lower concentrations, the hemorrhagic and/or proteolytic activities of four bothropic crude venoms (*B. jararacussu*, *Bothrops neuwiedi*, *B. moojeni* and *B. alternatus*) and two isolated SVMPs (P-III class BjussuMP-I from *B. jararacussu* and P-I class neuwiedase from *B. neuwiedi*).

Additionally, docking and molecular dynamics simulations involving BjussuMP-II, a P-I SVMP from *B. jararacussu* venom [39] with a very well characterized proteolytic activity, and Q8 compound were performed to get some insights into the inhibitory activity of this novel 4-quinolinone molecule against the action of SVMPs. These theoretical studies are justified since proteolysis is a common feature of SVMPs related to local tissue damage and hemorrhage. Therefore, the structural basis related to the harmful activities of the SVMP catalytic domains is a important topic for the identification of potential compounds for snake envenomation treatment.

2. Materials and methods

2.1. Materials and chemicals

All commercially available reagents were purchased from Aldrich Chemical Co. Reagents® and solvents were purified when necessary according to the usual procedures described in the literature. *B. jararacussu*, *B. neuwiedi*, *B. moojeni* and *B. alternatus* venoms were purchased from Bioagents Serpentarium Ltda. (Batatais, São Paulo State, Brazil). The SVMPs (P-III class BjussuMP-I, P-I class BjussuMP-II and P-I class neuwiedase) were isolated and biochemically characterized as previously described [39–41]. The licenses for scientific purposes are from *Instituto Brasileiro do Meio Ambiente e dos Recursos Naturais Renováveis – IBAMA* and *Instituto Chico Mendes de Conservação da Biodiversidade – ICMBio*. Numbers: 11094-2, 11094-1, 10394-1 and 15484-1.

The infrared spectra were measured on a Bomem M102® spectrometer (4000 - 400 cm^{-1}). NMR data assignment was based on ^{1}H and ^{13}C and the spectra were recorded on a Bruker DRX-200® and ARX-400®. Mass spectral analyses were carried out with a Shimadzu GCMS-QP5000® spectrophotometer. Analytical thin-layer chromatography was performed on a 0.25 mm film of silica gel containing a fluorescent indicator UV_{254} supported on aluminum sheet (Sigma–Aldrich®). Flash column chromatography was executed using a silica gel (Kieselgel 60, 230–400 mesh, E. Merck®). Gas chromatography was performed in a Shimadzu GC-17A® chromatograph equipped with a DB-5 column, employing H_2 as a carrier. Elemental analyses and the melting points were performed, respectively, with Fisons EA1108 CHNS-O® analyzer and FISATOM 430® equipment. Melting points were determined using a Microquimica MQAPF-301® device.

2.2. Compounds and procedures employed for 2-hydroxymethyl-6-methoxy-1,4-dihydro-4-quinolinone (Q8) synthesis

2.2.1. General procedure for the synthesis of enamines

In a flask under N_2 at 55 °C containing aniline (5.0 g, 0.054 mol) or *p*-anisidine (5.0 g, 0.041 mol) in dry methanol (1 mL/mmol aniline), DMAD (1 eq.) was added and the mixture was stirred overnight. Then methanol was removed under reduced pressure, and CH_2Cl_2 (30 mL) was added followed by a saturated solution of NH_4Cl (3 × 5 mL). The organic layer was dried over anhydrous $MgSO_4$, and evaporated to dryness under reduced pressure. The residue was purified on a silica gel column, using hexane:ethyl acetate 9.5:0.5 as eluent to afford desired enamine compounds 3 or 4 in 50% yield.

*2.2.1.1. 2-Phenylamino-2-enediocic acid dimethyl ester (compound **3**).* 6.3 g. IR (ν_{max}, film, cm^{-1}): 3457; 3380; 2953; 1739; 1668; 1282; 1031. ^{1}H NMR (200 MHz, $CDCl_3$): δ 9.67 (sl, 1H); 7.32–7.25 (m, 2H); 7.13–7.05 (m, 1H); 6.9 (m, 2H); 5.39 (s, 1H); 3.74 (s; 3H); 3.70 (s, 3H). ^{13}C NMR (50 MHz, $CDCl_3$) δ: 169.8; 164.7; 147.9; 140.2; 129.0; 124.1; 120.6; 116.6; 93.5; 52.6; 51.1. MS (% rel. intensity) *m/z*: 235.25 (6.9%); 144.15 (93.3%); 77.10 (100%).

*2.2.1.2. 2-(4-Methoxy-phenylamino)-2-enediocic acid dimethyl ester (compound **4**).* 5.5 g. IR (ν_{max}, film, cm^{-1}): 3284; 3210; 2952; 2836; 1742; 1637; 1033. ^{1}H NMR (200 MHz, $CDCl_3$): δ. 9.57 (sl, 1H); 6.91–679 (m, 4H); 5.30 (s, 1H); 3.78 (s, 3H); 3.73 (s, 3H); 3.67 (s, 3H). ^{13}C NMR (50 MHz, $CDCl_3$) δ: 182.4; 170.0; 164.8; 156.9; 149.0;

133.4; 123.0; 114.3; 91.7; 55.4; 52.6; 21.0. MS (% rel. intensity) *m/z*: 265.50 (12.6%); 146.15 (74.6%); 77.15 (96.5%).

*2.2.2. General procedure for the synthesis of 4-quinolinone compounds **5** and **6***

A flask adapted with a condenser containing diphenyl ether (8 mL) was heated in a sand bath up to the reflux temperature and then enamine compounds 3 or 4 (1.0 g) were added. The mixture was stirred for 10 min and transferred to an ice bath. The residue was purified by dry flash chromatography using a hexane – methylene chloride – MeOH gradient to afford the desired 4-quinolinone compounds 5 or 6 in 70% yield.

*2.2.2.1. Methyl-4-oxo-1,4-dihydroquinolinone 2-carboxylate (compound **5**).* 0.6 g mp: 215–217 °C. IR (ν_{max}, film, cm^{-1}): 3436; 2925; 2886; 1733; 1639; 1538; 1033. ^1H NMR (200 MHz, $CDCl_3$): 12.03 (s, 1H); 8.13 (d, J = 8.0 Hz, 1H); 7.95 (d, J = 10 Hz, 1H); 7.66–7.63 (m, 1H); 7.35–7.32 (m, 1H); 6.73 (s; 1H); 3.99 (s; 3H). ^{13}C NMR (50 MHz, $CDCl_3$) δ: 176.4; 161.1; 138.4; 135.8; 130.6; 124.4; 123.0; 122.1; 117.9; 108.8; 51.5. MS (% rel. intensity) *m/z*: 203 (30.1%); 143 (100%); 115.15 (72.9%); 89.15 (66.2%).

*2.2.2.2. Methyl-6-methoxy-4-oxo-1,4-dihydro-quinolinone carboxylate (compound **6**).* 0.53 g mp: 250–253 °C. IR (ν_{max}, film, cm^{-1}): 3440; 2935; 2865; 1729; 1639; 1552; 1024. ^1H NMR (200 MHz, $CDCl_3$): δ 12.14 (s, 1H); 7.92 (d, J = 9.1 Hz, 1H); 77.46 (d, J = 2.8 Hz, 1H); 7.37 (dd, J = 9.0, 2.8 Hz, 1H); 6.67 (s; 1H); 3.96 (s; 3H); 3.85 (s; 3H). ^{13}C NMR (50 MHz, $CDCl_3$) δ: 176.3; 162.3; 155.8; 136.2; 134.2; 126.7; 122.8; 120.9; 108.3; 103.2; 54.9; 52.9. MS (% rel. intensity) *m/z*: 207.50 (54.5%); 173.2 (91%); 73.2 (100%).

*2.2.3. General procedure for the synthesis of 4-quinolinone compounds **7** and **8***

In a flask containing 4-quinolinone compounds 5 or 6 (0.50 g) in dry THF (10 mL) under N_2 at 0 °C, $BH_3.SMe_2$ (1 eq) was added drop wise. The mixture was allowed to warm to room temperature overnight. Then dry methanol (3 × 10 mL) was added, the solvent was evaporated under atmospheric pressure and the crude product was recrystallized to furnish 4-quinolinone compounds 7 or 8 in 70% yield.

*2.2.3.1. 2-Hydroxymethyl-1,4-dihydro-4-quinolinone (compound **7**).* 0.3 g mp: 230–232 °C. IR (ν_{max}, film, cm^{-1}): 3384; 2946; 2917; 1619; 1359; 1083. ^1H NMR (200 MHz, $CDCl_3$): δ. 8.04 (dd, J = 8, 1 Hz, 1H); 7.69–7.56 (m, 2H); 7.31–7.23 (m, 1H); 6.02 (s, 1H); 4.48 (s, 2H).^{13}C NMR (50 MHz, $CDCl_3$) δ: 153.5; 140.4; 131.6; 125.3; 125.0; 122.9; 118.6; 105.6; 60.5. Anal. Calcd for $C_{10}H_9NO_2$:C, 68.56%; H, 5.18%; N, 8.0%. Found: C, 68.60%; H, 5.18%; N, 7.90%.

*2.2.3.2. 2-Hydroxymethyl-6-methoxy-1,4-dihydro-4-quinolinone (compound **8** or Q8).* 0.3 g mp: 250–252 °C. IR (ν_{max}, film, cm^{-1}): 3448; 2921; 2852; 1637; 1504; 1035. ^1H NMR (200 MHz, $CDCl_3$): δ 7.94 (dd, J = 8.4.1 Hz, 1H); 7.52–7.41 (m, 2H); 6.63 (s, 1H); 4.72 (s, 2H); 3.89 (s, 3H).^{13}C NMR (50 MHz, $CDCl_3$) δ: 171.5; 156.8; 155.5; 134.5; 124.2; 123.2; 121.0; 103.1; 102.7; 60.0; 55.6. Anal. Calcd. for $C_{11}H_{11}NO_3$: C, 64.38%; H, 5.4%; N, 6.83%. Found: C, 64.41%; H, 5.55%; N, 6.81%.

*2.2.4. General procedure for the synthesis of quinolines **9**, **10** and **11***

To a flask containing compound **6** or **8** (0.1 mmol) and K_2CO_3 (20.7 mg, 0.15 mmol) it was added anhydrous DMF (50 μL) and ethyl bromide (9.5 μL, 0.15 mmol). The flask was stirred for 12 h at room temperature. The solution was filtered in silica to remove the precipitate and the solvent was evaporated, then the resulting material was purified by column chromatography in silica gel using a gradient of n-hexane – methanol as eluent furnishing products **9** and **10** in 80% yield.

*2.2.4.1. 4-ethoxy-6-methoxy-2-quinoline methyl carboxylate (compound **9**).* 17 mg mp: 105–107 °C. IR (ν_{max}, KBr) cm^{-1}: 2933; 2856; 1730; 1639; 1483; 1236; 1024. ^1H NMR (400 MHz, $CDCl_3$) δ: 8.11 (d, J = 9.2 Hz, 1H); 7.55 (s, 1H); 7.46 (d, J = 2.8 Hz, 1H); 7.48 (dd, J = 9.2, 2.8 Hz, 2H); 4.36 (q, J = 7 Hz, 2H); 4.06 (s, 3H); 3.96 (s, 3H); 1.60 (t, J = 7 Hz, 3H). ^{13}C NMR (100 MHz, $CDCl_3$) δ: 166.46; 161.29; 158.91; 146.60; 144.42; 131.82; 123.42; 123.02; 101.01; 99.61; 64.53; 55.64; 53.08; 14.48.

*2.2.4.2. 4-ethoxy-6-methoxy-2-quinolilmethanol (compound **10**).* mp: 120–123 °C. IR (ν_{max}, KBr) cm^{-1}: 2947; 2866; 1643; 1592; 1382; 1031; 825. ^1H NMR (400 MHz, $CDCl_3$) δ: 7.77 (d, J = 9.14 Hz, 1H); 7.42 (d, J = 2.7 Hz, 1H); 7.32 (dd, J = 9.2, 2.9 Hz, 1H); 7.55 (s, 1H); 4.75 (s, 2H); 4.31 (q, J = 7.0 Hz, 2H); 3.88 (s, 3H); 1.55 (t, J = 7 Hz, 3H). ^{13}C NMR (100 MHz, $CDCl_3$) δ: 162.11; 161.19; 157.41; 144.63; 130.72; 122.52; 121.52; 100.73; 99.72; 65.86; 64.91; 56.35; 15.33.

*2.2.4.3. 4-ethoxy-2-ethoxymethyl-6-methoxyquinoline (compound **11**).* In a suspension of NaH 60% (3 mg, 0.077 mmol) in dry DMF (100 μL) and DME (500 μL) was added a solution of compound **8** (15 mg, 0.064 mmol) in DME (100 μL) at 0 °C. After 10 min the mixture was treated with LiBr (12 mg, 0.128 mmol) and stirred by 15 min. Then ethyl bromide was added (8.3 mg, 0.077 mmol) dropwise. The mixture was stirred at room temperature by 3 h; after ice addition, it was extracted with ethyl acetate (3 × 10 mL) and the combined organic phases where washed with brine (3 × 5 mL). The resulting solution was dried with anhydrous sodium sulfate and the solvent was evaporated. The crude material was purified using column chromatography in silica gel with hexane:ethyl acetate 6:4 as eluent. Compound 11 was obtained in 80% yield (13.3 mg). mp: 69–72 °C. IR (ν_{max}, KBr) cm^{-1}: 2975; 2931; 2886; 1704; 1596; 1224; 1093; 831. ^1H NMR (400 MHz, $CDCl_3$) δ: 7.88 (d, J = 9.1 Hz, 1H); 7.44 (d, J = 2.8 Hz, 1H); 7.32 (dd, J = 9.1, 2.8 Hz, 1H); 6.94 (s, 1H); 4.71 (s, 2H); 4.30 (q, J = 7.0 Hz, 2H); 3.93 (s, 3H); 3.64 (q, J = 7 Hz, 2H), 1.57 (t, J = 7 Hz, 3H), 1.29 (t, J = 7 Hz, 3H). ^{13}C NMR (100 MHz, $CDCl_3$) δ: 161.27; 158.11; 157.12; 144.39; 129.92; 121.97; 99.98; 98.82; 74.39; 66.35; 64.09; 55.56; 15.28; 14.55.

2.3. Biological assays

Animal procedures were in accordance with the guidelines for animal care prepared by the Committee on Care and Use of Laboratory Animal Resources, National Research Council, USA. Animal care was in accordance with the guidelines of the Brazilian College for Animal Experimentation (COBEA) and was approved by Committee for Ethics in Animals Utilization of USP/Campus Ribeirão Preto-SP (Process n° 07.1.517.53.6).

2.3.1. Hemorrhagic activity

50 μg of desiccated crude venoms (*B. jararacussu*, *B. moojeni* and *B. alternatus*) and freeze-dried SVMP BjussuMP-I from *B. jararacussu* were weighed and dissolved in phosphate-buffered saline (PBS, pH 7.2), while the synthetic compounds, named 5 through 11 were dissolved in DMSO, including the compound of interest, Q8. For the initial screening, Swiss male mice (18–22 g, n = 6) were injected intradermically (50 μL) in the back region with different pre-incubated (30 min; 37 °C) doses containing different crude venoms/SVMPs:5 through 11 compounds at a 1:10 proportion (w/w). Control mice received PBS or DMSO. Three hours after injection, the mice were sacrificed and the diameter of the hemorrhagic spot on the back skin was measured [39,40].

After selecting the compound Q8, a hemorrhagic activity inhibition test was performed, (i) one with pre-incubation (30 min; 37 °C) of the venoms/metalloproteases with different doses of the compound Q8 (1:5, 1:10, 1:15 and 1:30, w/w); and (ii) a post-envenoming test, where first the mice only received intradermal injections containing BjussuMP-I (50 μg/50 μL), and after 15 min, the same animals were inoculated by the same route with the compound Q8 in the proportions 1:30 and 1:100 (SVMP: Q8, w/w). The assessment of the hemorrhagic activity was conducted in the same manner and three hours after injection, mice were killed and the diameter of the hemorrhage zone in the skin was measured.

2.3.2. Proteolytic activity on casein

40 μg of crude snake venoms (*B. jararacussu* and *B. neuwiedi*) or SVMPs BjussuMP-I from *B. jararacussu* and neuwiedase from *B. neuwiedi* previously incubated with Q8 at different w/w ratios (1:5, 1:10, 1:15 and 1:30), were incubated with 1.0 mL of 1% (w/v) casein in 0.1 M Tris–HCl buffer (pH 8.0) for 30 min at 37 °C. The reaction was blocked by the addition of 1.0 mL of 5% (v/v) trichloroacetic acid solution and the mixture remained at room temperature for 30 min before centrifugation (2000 × *g*) for 5 min at 25 °C. Proteolytic activity was estimated by monitoring the absorbance of the clear supernatant at 280 nm [39,40].

2.3.3. Statistical analysis

Results are presented as the mean value ± SD obtained with the indicated number of tested animals. The statistical significance of differences between groups was evaluated using Student's unpaired t-test. A P value < 0.05 was considered to indicate significance.

2.4. Computational procedures

2.4.1. BjussuMP-II modeling

According to the alignment data from the based-threading method program HHpred [42], available at the Max-Planck Institute for Developmental Biology server (http://toolkit.tuebingen.mpg.de/hhpred), a 1.05 Å resolution crystallographic model of the zinc metalloproteinase BaP1 from *Bothrops asper* snake venom complexed to a peptidomimetic inhibitor [43] (PDB code 2w15) was selected as a template for the construction of the native P-I class BjussuMP-II structural model. This template, selected in the Protein Data Base (PDB) using the algorithm BlastP (*default* parameters), was chosen based on the alignment score (337.81) and its identity (81%) to the BaP1 sequence. The program Modeller 9v10 [44] was then used to generate ten structural models based on the selected template, keeping the original position of the cofactor Zn^{2+}. Additionally, the 1.93 Å resolution crystallographic model of the native zinc metalloproteinase BaP1 [45] from *Bothrops asper* (PDB code 1nd1) was also added to the Modeller 9v10 alignment input to define the position of the Glu42/Zn^{2+}-coordinated catalytic water molecule in the generated models. Variable target function method (VTFM) with conjugate gradients (CG) [44] and molecular dynamics (MD) [44] with simulated annealing (SA) [44] were used in order to refine the models. The Zn^{2+} cofactor of each model was added based on the coordinates of this ion in the BaP1/peptidomimetic inhibitor crystallographic model. The best BjussuMP-II model was selected according to the stereochemical and energy parameters determined respectively by the programs RAMPAGE [46] and ProSA-web [47].

2.4.2. Q8 in silico design and docking simulations

The program Avogadro v.0.9.4 [48] was used to design Q8 and improve its overall structure by an energy minimization process based on the MMF94 force field and in a steepest-descent algorithm. All docking simulations between the native BjussuMP-II model and the ligand were executed by the program Gold v.5.0.1 (CCDC Software Limited, Cambridge, U.K.) [49]. The docking site was defined within a 20 Å radius around the cofactor Zn^{2+} localized at the protein active site. The docking simulations were performed with the options on/fix, on/spin, toggle/fix and toggle/spin to evaluate the influence of the Glu142/Zn^{2+}-coordinated catalytic water molecule on the docking solutions. A minimum of ten rounds were executed for each simulation, with the generation of twenty docking solutions per round; the other docking parameters were defined according to the GOLD v.5.0.1 default settings. The docking solutions between Q8 and the native BjussuMP-II model were scored using the GoldScore fitness functions [49].

2.4.3. Molecular dynamics simulations

The BjussuMP-II/Q8 docking solutions which presented the highest GoldScore values were submitted to molecular dynamics (MD) simulations using the program GROMACS (Groningen Machine for Chemical Simulation) v.4.5.4 [50,51]. The GROMOS 96 53a6 force field [52] was chosen to perform the MD simulations and the protonation states of the charged groups were set to pH 7.0. All the MD simulations were executed in the presence of explicit water molecules [53] and the minimum allowed distance between any atom of the models and the box wall was set to 1.0 nm. An energy minimization (EM) using a steepest descent algorithm was performed to generate the starting configuration of the systems. After this step, 200 ps of MD simulation with position restraints applied to the protein (PRMD) was executed in order to relax the systems gently. Then, 15 ns of unrestrained MD simulation were calculated to evaluate the stability of the structures. All MD simulations were carried out in a periodic truncated cubic box under constant temperature (298 K) and pressure (1.0 bar), which were held by coupling to an isotropic pressure and external heat bath [54]. The distances between the catalytic histidines and the Zn^{2+} ion of the native BjussuMP-II model and the BjussuMP-II/Q8 complexes were kept according to Andreini et al. [55]. Q8 topology and coordinates files used for molecular dynamics (MD) simulations were generated by the Dundee PRODRG2 Server (http://davapc1.bioch.dundee.ac.uk/prodrg/).

2.4.4. Evaluation of the theoretical structural models

Overall stereochemical and energy quality of the native BjussuMP-II model and the BjussuMP-II/Q8 complex after their respective MD simulations were checked with the programs RAMPAGE [46] and ProSA-web [47]. Additionally, in order to assess the quality of the native BjussuMP-II model and BjussuMP-II/Q8 complex after their respective MD simulations, the average rmsd (root mean square deviation)/time graph of the protein backbone atoms were analyzed in terms of the difference between the total averages of two equal sets of points (the transient part of the MD simulations was not considered).

3. Results and discussion

3.1. Synthesis of 2-hydroxymethyl-6-methoxy-1,4-dihydro-4-quinolinone (Q8)

The synthetic route to obtain 2-hydroxymethyl-6-methoxy-1,4-dihydro-4-quinolinone (Q**8**) from a commercially available anisiline in three steps is shown in Fig. 1. The first step involves an enamine bond formation, which was achieved in 80% yield through condensation of dimethyl acetylenodicarboxylate (DMAD) with the anisiline compound 2, as described by Edmont [56]. Intramolecular cyclization to obtain the compound 4 was performed under reflux in different conditions and the best results were obtained with 70%

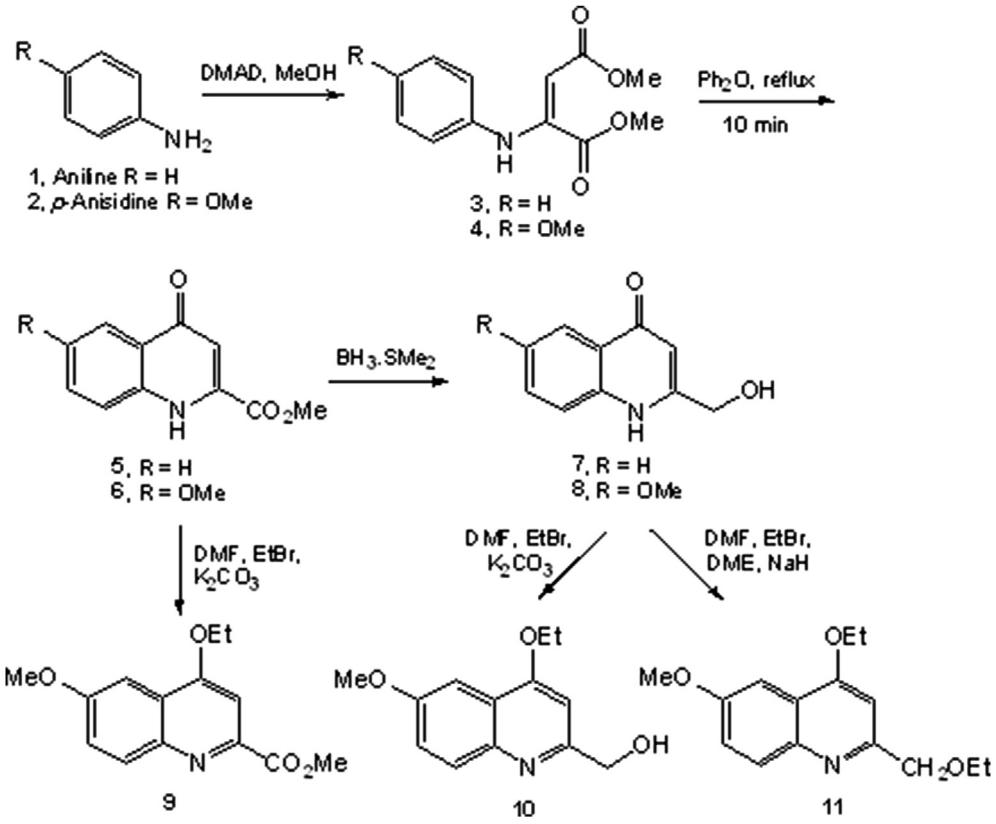

Fig. 1. Synthetic route to obtain 2-Hydroxymethyl-6-methoxy-1,4-dihydro-4-quinolinone (Q8) (1).

yield. Initially, the solvent diphenylether (DFE) was heated to reflux and afterwards enamine compound 3 was added and refluxed during 10 min. In order to completely stop the reaction and avoiding decomposition of the desired product, the flask was immediately transferred to an ice bath. The purification of quinolinone compound 4 was achieved using dry flash with a hexane/methylene chloride/methanol solvent gradient. The chemoselective reduction of quinolinone compound 4 was carried out with $BH_3.SMe_2$, furnishing compound 8 or Q8 in good yield (~70%). Infrared and NMR data assays were used to confirm the identity of the Q8 compound (section 2.2.3).

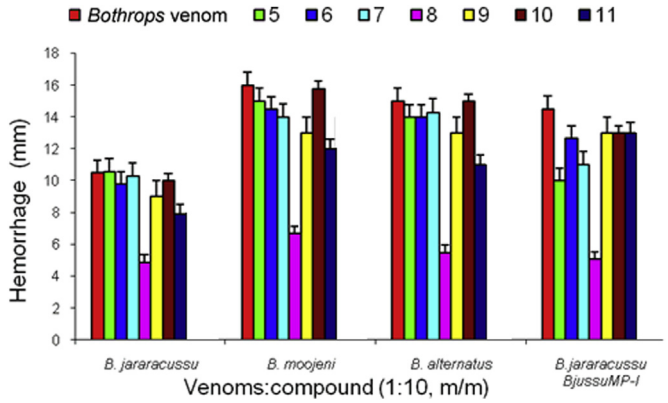

Fig. 2. Screening all quinolinones versus crude venoms or BjussuMP-I. Effect quinolinones (compounds 5–11) on the hemorrhage induced by *Bothrops* snake venoms (*B. moojeni*, *B. jararacussu* and *B. alternatus*) and BjussuMP-I, a SVMP from *B. jararacussu* venom.

3.2. Biochemical/pharmacological trials with Q8 demonstrated its high inhibitory efficacy against crude snake venoms and SVMPs

Fig. 2 shows the initial screening of quinolinones (compounds Q5–Q13) against crude bothropic venoms and BjussuMP-I at 1:10 w/w proportions (crude bothropic venoms/BjussuMP-I:quinolinone). These assays showed clearly that the molecule Q8 is the most effective hemorrhagic inhibitor compared to the other quinolinones. Taking into account the remarkable inhibitory activity of the Q8 molecule, a further *in vivo* hemorrhagic experiment was performed using pre-incubated mixtures containing different crude bothropic venoms/BjussuMP-I:Q8 w/w proportions (Fig. 3A). In this experiment, the crude snake venoms and BjussuMP-I which were not pre-incubated with Q8 induced hemorrhagic spots varying from 8 to 13 mm of diameter in the back skin of the mice. In contrast, after pre-incubation with the quinolinone compound, the hemorrhagic spot in the back skin of the mice was clearly reduced even considering the 1:5 w/w proportion (crude venom/BjussuMP-I:Q8). At the minimum inhibitor proportion (1:5 w/w), the hemorrhagic spot diameter was, on average, around 6 mm (25% reduction), 7 mm (42% reduction), 10 mm (23% reduction) and 5 mm (45% reduction) respectively for *B. jararacussu*, *B. moojeni*, *B. alternatus* crude venoms and BjussuMP-I from *B. jararacussu*. The increase in the amount of Q8 in relation to crude venoms or BjussuMP-I showed a progressive inhibition potency, culminating in a reduction of approximately 81.25% (~1 mm diameter), 87.5% (~1 mm diameter), 76.9% (~3 mm diameter) and 77.8% (~2 mm diameter) in the diameter of induced hemorrhagic spots, respectively, by *B. jararacussu*, *B. moojeni* and *B. alternatus* crude venoms and BjussuMP-I after pre-incubation with the maximum Q8 proportion (1:30 w/w). Additionally, a post-envenoming experiment confirmed the compound Q8 was also able to inhibit the formation

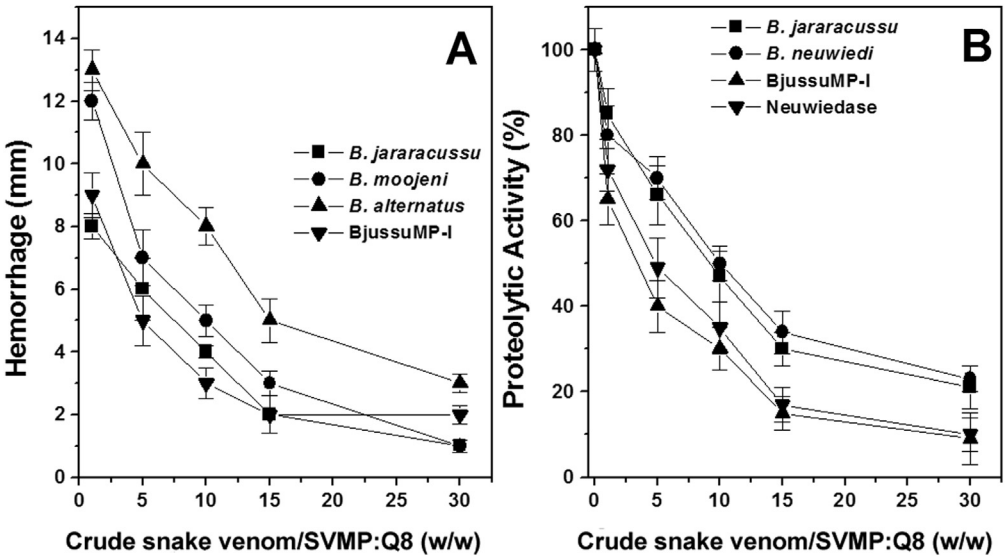

Fig. 3. (A) Effect of 2-Hydroxymethyl-6-methoxy-1,4-dihydro-4-quinolinone (Q8) on the hemorrhage induced by *Bothrops* snake venoms (*B. moojeni*, *B. jararacussu* and *B. alternatus*) and BjussuMP-I, a SVMP from *B. jararacussu* venom. The hemorrhagic spots on the back skin of mice were measured 3 h after intradermic injection of the crude venoms or SVMP pre-incubated with the Q8 (30 min, 37 °C) at different crude venom/BjussuMP-I:Q8 w/w ratios (1:5, 1:10, 1:15 and 1:30). In the control experiments (shown at left of the graph), mice received PBS or DMSO. Results are expressed as mean ± S.D. (n = 6). (B) Effect of Q8 on the proteolytic activity on casein induced by *Bothrops* snake venoms (*B. jararacussu* and *B. neuwiedi*) and isolated SVMPs BjussuMP-I and neuwiedase from *B. jararacussu* and *B. neuwiedi* venoms, respectively. Different crude venom/SVMP: Q8 w/w ratios (1:5, 1:10, 1:15 and 1:30) were tested to assay the Q8 inhibitory activity using a 1.0 mL 1% (w/v) casein solution. The measurements were performed after incubation (30 min, 37 °C) and the proteolytic activity was estimated monitoring the absorbance of the supernatant at 280 nm at different. The control experiments are shown at left of the graph. Results are expressed as mean ± S.D. (n = 6).

of the hemorrhagic spots induced by BjussuMP-I. The results of this assay indicated a significant reduction of the hemorrhagic activity when Q8 was administered at 1:30 and 1:100 w/w (toxin/Q8) proportions after 15 min of the BjussuMP-I injection (47% and 66%, respectively).

Proteolytic activity of *B. jararacussu* and *B. neuwiedi* crude venoms and the SVMPs BjussuMP-I and neuwiedase on casein was also inhibited significantly by Q8. In Fig. 3B, it is possible to observe that the proteolytic activity of the control experiments (performed without pre-incubation with Q8) presented an efficiency superior to 60% for all tested crude venoms or SVMPs. In contrast, after pre-incubation with the inhibitor, the efficiency of the proteolytic activity dropped to values near 20% and 10%, respectively, for crude venoms and SVMPs.

Therefore, the data above show that Q8 can inhibit efficiently the hemorrhagic activity of some crude snake venoms and isolated the SVMP BjussuMP-I from *B. jararacussu* in mice. Additionally, the same conclusion can be drawn from experiments involving proteolytic activity on casein of tested crude venoms and SVMPs. These findings indicate the potential of Q8 as an anti-snake venom drug, particularly for the treatment of the hemorrhagic and necrotic effects induced by the action of snake venoms and SVMPs found in these complex biological mixtures.

3.3. Structural insights into BjussuMP-II inhibition by Q8

3.3.1. BjussuMP-II structural model

According to the biochemical trials, Q8 was particularly efficient in the inhibition of hemorrhagic and proteolytic activities induced by some crude snake venoms and snake venom metalloproteases (SVMPs). These results suggest that the toxin and Q8 interactions could be circumscribed to the active site and/or surroundings of SVMPs, since the catalytic domains of these toxins are related to these harmful pharmacological and biological properties. Hence, docking and molecular dynamics simulations involving a theoretical model of a P-I class SVMP, which is constituted by a single catalytic domain (present and conserved in all SVMPs), and Q8 were performed in order to provide noteworthy insights into the structural features of this and other similar complexes.

Initial theoretical model of the native BjussuMP-II SVMP was built [42,44] using two crystallographic models as templates: a zinc metalloproteinase BaP1 from *B. asper* snake venom complexed to a peptidomimetic inhibitor [43] and a native metalloprotease BaP1 from *B. asper* [45]. This protein presents an identity degree of 81% in relation to BjussuMP-II and the score of the alignment between these two sequences was 417.0 [42]. The initial theoretical model of the native BjussuMP-II was then improved through a 20 ns-MD simulation [50,51] and it presented, after 5000 ps, a maximum rmsd backbone atom amplitude of approximately 1.0 Å and a rmsd backbone atom average difference around 0.1 Å between 5001-12500 ps and 12501–20000 ps (the first transient 5000 ps was not considered). After the MD simulation, the final model of the native BjussuMP-II showed a good stereochemical quality: 96.1% of its residues were in the core and additionally allowed regions of the Ramachandran plot [46] and the potential energy of the entire structure presented a negative balance (Z-score = - 6.52) [47].

Based on the data showed above, it is possible to suppose that the theoretical native BjussuMP-II model obtained after the 20 ns-MD simulation is feasible, not showing an apparent structural instability. The model obtained at the end of the 20 ns-MD simulation also kept the structural similarity in relation to other experimentally-determined SVMP catalytic domains [57–64], presenting three disulfide bridges (Cys116-Cys196, Cys156-Cys180, and Cys158-Cys163) and two ellipsoidal subdomains: the major one containing the first 152 residues (four α-helices – A, B, C, and D, and six stranded β-sheets – sI, sII, sIII, sIV, sV, and sVI) and the minor one enclosing the remaining 98 residues (one α-helix and several loops). Additionally, the imidazole rings from catalytic histidines presented a favorable position to coordinate the catalytic zinc after the 20 ns-MD simulation, reinforcing the probable

adequate structural conformation of the final native BjussuMP-II model. Likewise, the side chain of the residue Glu142, which is also essential for the nucleophilic attack on the scissile peptide bond of metalloproteinase substrates [57], also remained in the vicinity of the catalytic histidines.

3.3.2. *BjussuMP-II/Q8 complex model and its comparison with other complexed-SVMP structures*

Following the 20 ns-MD simulation, a molecular docking simulation was carried out with the final native BjussuMP-II model and Q8. For this purpose, the docking site of the ligand was defined as a sphere of approximately 4000 Å^3 around the BjussuMP-II catalytic ion Zn^{2+}. The definition of the active site and its surroundings as the docking site was based on several crystallographic experiments which indicate that these protein spots are effectively the regions of interaction between different SVMPs and specific inhibitors or ligands. In 1994, Zhang et al. [59], solved crystallographic complexes between atrolysin C (form d), a SVMP from *Crotalus atrox* venom, and the natural PyroGlu-Asn-Trp tripeptide and synthetic SCH47890 ligands, demonstrating that these molecules bind to the atrolysin C active site region. Similarly, Cirilli et al. [65], solved the adamalysin II from *Crotalus adamanteus* crystallographic structure bound to an analogue of POL647, a synthetic tripeptide derivative from the natural reprolysin inhibitors found in crotalid and viperid snake venoms, and showed that the ligand interacts with catalytic site residues and the cofactor Zn^{2+} in an asymmetric bidentate, partly filling the primary specificity subsite S1'. Furthermore, the presence of the inhibitor in this complex displaces the catalytically essential water molecule, which is coordinated by the cofactor Zn^{2+} and a glutamate residue in the native protein. The non-covalent interaction of other peptidomimetic inhibitors (POL647 and POL656) with residues of the adamalysin II active site region was also described by Gomis-Rüth et al. [58]. Analyzing the potential contributions of the adamalysin II/POL647 and adamalysin II/POL656 complexes for drug design of TACE (TNFα-converting enzymes) inhibitors, the authors indicated that the insertion of these inhibitors in the adamalysin II active site provoked a slight opening of the substrate-binding cleft, as also described by Zhang et al. [61] in the complex tripeptide KNL/SVMP F-II from *Agkistrodon acutus*.

Our molecular docking results showed that the best protein/ligand solutions (GoldScore Fitness ≅ 55) present similar orientations of Q8, which are deeply inserted into the S_1'-pocket of the native BjussuMP-II model, occupying a region nearby the helix D, β-strand sIV, and bulged segment (a region anterior to the β-strand sIV edge which protrudes into the active site cleft) (for a complete description of the SVMP structural elements see the review prepared by Stöcker et al. [66]). Interestingly, the analysis of these molecular docking solutions seem to indicate that the fitting of the inhibitor does not necessarily implicate in a displacement of the Glu142/Zn^{2+}-coordinated catalytic water molecule, thus indicating that the inhibitory activity of Q8 is probably not linked to the impairment of the dyad Glu142/reactive solvent molecule. Therefore, according to the molecular docking simulation, the ligand could just impair the correct contact between the components of the catalytic site and substrate molecules, not allowing the occurrence of any hydrolytic reaction due to a considerable steric hindrance.

In order to verify the feasibility of these results, the BjussuMP-II/Q8 molecular docking solution with the highest score (GoldScore Fitness ≅ 55.12) was submitted to an extended MD simulation (50 ns) to assess the stability of this complex and identify the prevalence of possible protein/inhibitor interactions. The analysis of the BjussuMP-II/Q8 structure after the 50 ns-MD simulation showed a maximum rmsd backbone atom amplitude of approximately 0.8 Å and a rmsd backbone atom average difference around 0.1 Å between 2001–24000 ps and 24001–50000 ps (the first transient 2000 ps was not considered). Consequently, as in the first 20 ns-MD simulation, it is possible to assume that the model of the protein/inhibitor complex does not present an instability tendency during the 50 ns-MD simulation. In addition, after this 50 ns-MD simulation, the general stereochemistry quality (97.1% of the residues were in the core and additionally allowed regions of the Ramachandran plot) (46) and potential energy (47) (Z-score = -6.27) were essentially kept in comparison to the initial model obtained after the 20 ns-MD simulation.

Indeed, the data from the latter MD simulation revealed more interesting features which could shed some light on the structural basis related to the SVMP inhibitory activity of Q8. An analysis of the interactions between ligand and protein during the 50 ns-MD simulation indicated that the formation of hydrogen bonds seems not to play an essential role for the stabilization of the BjussuMP-II/Q8 complex. The most prevalent hydrogen bond (formed between the Q8 hydroxymethyl group and the Gln108 Nε2 atom) occurred during only approximately 5.5% of the MD simulation (~2.75 ns), whereas none of the remaining exceeded 1.5% (~0.75 ns). On the other hand, an important interaction involving the oxygen atom from the Q8 carbonyl group and the cofactor Zn^{2+} is observed in the BjussuMP-II/Q8 complex, since an average distance of 1.9 Å was kept between these atoms during all the 50 ns-MD simulation (Fig. 4).

In fact, according to the program FindGeo [67], Q8 takes part in a regular square pyramidal coordination of the cofactor Zn^{2+}, which is completed by the Nε2 atoms from active site histidines and the Glu142/Zn^{2+}-coordinated catalytic water molecule and presents a rmsd value of only 0.312 Å in relation to the ideal geometry of this type of coordination. Interestingly, the Zn^{2+} regular square coordination found in the BjussuMP-II/Q8 complex is unique in comparison to the total of 27 native or ligand-complexed SVMP crystal structures currently available in PDB (Protein Data Bank). This finding, associated with the fact that this ligand apparently binds to BjussuMP-II without displacing the Glu142/Zn^{2+}-coordinated

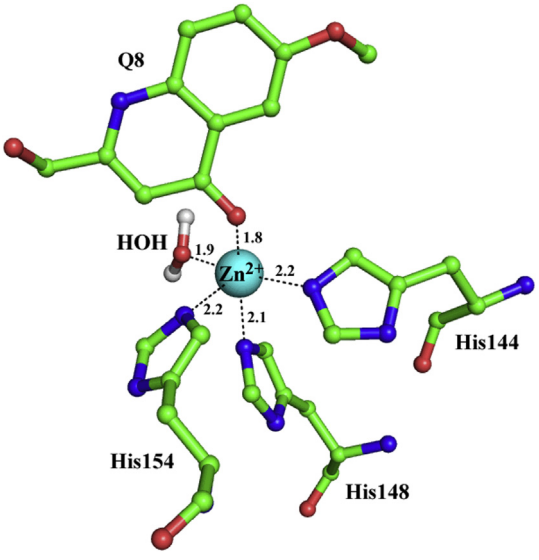

Fig. 4. BjussuMP-II/Q8 interactions. An average distance of 1.9 Å was kept between the oxygen atom from Q8 carbonyl group and the cofactor Zn^{2+} during the 50 ns-MD simulation. The distances (Å) from the catalytic histidines (His144, His148, and His154) and Glu142/Zn^{2+}-coordinated catalytic water molecule (HOH) to the cofactor Zn^{2+} are also shown to attest the appropriate conformation of the active site after the 50 ns-MD simulation. This illustration was generated with program PyMOL v.1.3.

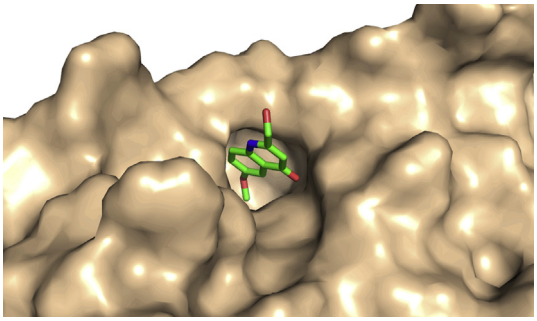

Fig. 5. Fit of Q8 (depicted in sticks) into the active site cavity of BjussuMP-II (depicted in a surface representation). The low molecular weight and shape of the synthetic molecule seem to be appropriate to provide an optimum access to the catalytic site, allowing the impairing of the SVMP activity possibly by a steric hindrance mechanism. This illustration was generated with program PyMOL v.1.3.

catalytic water as occurs in other available ligand-complexed SVMP crystal structure molecules, highlights the potential singular Q8 characteristics in relation to other SVMP inhibitors. A possible explanation for these features could be the low molecular weight (173 Da) of Q8 in comparison to other SVMP inhibitors. This compact shape of this synthetic quinolinone probably provides better access and an appropriate fit into the BjussuMP-II active site (Fig. 5), thus favoring the interaction between the carbonyl group from the inhibitor and the protein cofactor Zn^{2+}. Therefore, it is very plausible that Q8 is able to impair the SVMP activity by a steric hindrance mechanism related to its remarkable compact dimensions. Also, this low molecular weight probably is particularly useful for its application against local effects caused by ophidic venoms since it allows a rapid tissue diffusion. Indeed, our *in vivo* experiments support this last supposition given that the addition of Q8 helped to reduce significantly the myotoxic effect caused by *B. jararacussu* PLA_2s in mice.

Thereby, the structural analysis of the BjussuMP-II/Q8 model underscored the potential use of this synthetic quinolinone as an adjuvant in snakebite serum therapy, mainly in order to relieve the hemorrhagic and proteolytic actions of the *Bothrops* metalloproteases, as previously attested by the biological and functional assays. Moreover, future pharmacological and structural studies involving Q8 could also reveal more important clues for the development of structure-based drugs against defective homologue proteases involved in haemostatic system diseases which affect humans and other mammals.

4. Conclusions

The experimental results indicate that Q8 is able to inhibit significantly hemorrhagic and/or proteolytic activities presented by crude snake venoms from *B. jararacussu*, *B. moojeni* and *B. alternatus* and the isolated metalloproteases BjussuMP-I from *B. jararacussu* and neuwiedase from *B. neuwiedi* in mice. According to structural studies involving docking and molecular dynamics simulations, a possible explanation for the inhibitory properties of this quinolinone molecule could be its low molecular weight structure, which allows an appropriate fit into the BjussuMP-II active site. The formation of a stable complex between Q8 and BjussuMP-II or other SVMPs may, consequently, impair the access of substrates to the active site of these toxins, explaining thus the hemorrhagic and proteolytic inhibition verified in the experimental trials. Indeed, a detailed analysis of the contacts formed during the MD simulation between the residues from the BjussuMP-II active site and Q8 shows the carbonyl group from the inhibitor and the protein cofactor Zn^{2+} hold the main interaction responsible for the stabilization of the complex BjussuMP-II/Q8. Additionally, the low molecular weight of this quinolinone probably is potentially useful for application against local effects caused by ophidic venoms since this characteristic could permit rapid tissue diffusion of the inhibitor. Therefore, the experimental and theoretical data indicate that Q8 is an interesting drug-candidate compound for antiophidic therapy, particularly for the treatment of hemorrhagic and necrotic effects induced by the action of bothropic and other viperid snake venoms.

Conflict of interests

None.

Acknowledgments

The authors express their gratitude to Coordenação de Aperfeiçoamento de Pessoal de Nível Superior (CAPES), Conselho Nacional de Desenvolvimento Científico e Tecnológico (CNPq), Fundação de Amparo à Pesquisa do Estado de São Paulo (FAPESP), Fundação de Amparo à Pesquisa do Estado de Minas Gerais (FAPEMIG), Instituto Nacional de Ciência e Tecnologia em Toxinas (INCTTox) and Fundação de Amparo à Pesquisa do Estado de Rondônia (FAPERO) for the financial support, and to Conselho de Gestão do Patrimônio Genético (CGEN/MMA) for the authorization number 010627/2011-1. We also thank Prof. José R. Giglio (FMRP-USP, Brazil) (*in memorian*), Tássia R. Costa and Renata S. Fernandes (FCFRP-USP) for their academic advising. The authors thank the Program for Technological Development in Tools for Health-PDTIS-FIOCRUZ for use of its facilities. Amy Grabner provided the English editing of the manuscript.

References

[1] M. Risch, D.D. Georgieva, M.M. Von Bergen, N. Jehmlich, N. Genov, R.K. Arni, C. Betzel, Snake venomics of the siamese russell's viper (*Daboia russelli siamensis*) – relation to pharmacological activities, J. Proteomics 72 (2009) 256–269.

[2] D. Georgieva, M. Risch, A. Kardas, F. Buck, M. Von Bergen, C. Betzel, Comparative analysis of the venom proteomes of *Vipera ammodytes ammodytes* and *Vipera ammodytes meridionalis*, J. Proteome Res. 7 (2008) 866–886.

[3] L. Sanz, N. Ayvazyan, J.J. Calvete, Snake venomics of the Armenian mountain vipers *Macrovipera lebetina obtusa* and *Vipera raddei*, J. Proteomics 71 (2008) 198–209.

[4] J.J. Calvete, C. Marcinkiewicz, L. Sanz, Snake venomics of *Bitis gabonica gabonica*. Protein family composition, subunit organization of venom toxins, and characterization of dimeric disintegrins bitisgabonin-1 and bitisgabonin-2, J. Proteome Res. 6 (2007) 326–336.

[5] J.J. Calvete, E. Fasoli, L. Sanz, E. Boschetti, P.G. Righetti, Exploring the venom proteome of the western diamondback rattlesnake, *Crotalus atrox*, via snake venomics and combinatorial peptide ligand library approaches, J. Proteome Res. 8 (2009) 3055–3067.

[6] A. Alape-Giron, L. Sanz, J. Escolano, M. Flores-Diaz, M. Madrigal, M. Sasa, J.J. Calvete, Snake venomics of the lancehead pitviper *Bothrops asper*: geographic, individual, and ontogenetic variations, J. Proteome Res. 7 (2008) 3556–3571.

[7] A. Alape-Giron, M. Flores-Diaz, L. Sanz, M. Madrigal, J. Escolano, M. Sasa, J.J. Calvete, Studies on the venom proteome of *Bothrops asper*: perspectives and applications, Toxicon 54 (2009) 938–948.

[8] J.J. Calvete, L. Sanz, P. Cid, P. De La Torre, M. Flores-Diaz, M.C. Dos Santos, A. Borges, A. Bremo, Y. Angulo, B. Lomonte, A. Alape-Giron, J.M. Gutierrez, Snake venomics of the central American rattlesnake *Crotalus simus* and the South American *Crotalus durissus* complex points to neurotoxicity as an adaptive paedomorphic trend along crotalus dispersal in South America, J. Proteome Res. 9 (2010) 528–544.

[9] M. Ohler, D. Georgieva, J. Seifert, M. Von Bergen, R.K. Arni, N. Genov, C. Betzel, The venomics of *Bothrops alternatus* is a pool of acidic proteins with predominant hemorrhagic and coagulopathic activities, J. Proteome Res. 9 (2010) 2422–2437.

[10] A.T. Ching, M.M. Rocha, A.F. Paes Leme, D.C. Pimenta, D.F.M. De Fatima, S.M. Serrano, P.L. Ho, I.L. Junqueira-De-Azevedo, Some aspects of the venom proteome of the Colubridae snake *Philodryas olfersii* revealed from a Duvernoy's (venom) gland transcriptome, FEBS Lett. 580 (2006) 4417–4422.

[11] G. Ompraba, A. Chapeaurouge, R. Doley, K.R. Devi, P. Padmanaban, C. Venkatraman, D. Velmurugan, Q. Lin, R.M. Kini, Identification of a novel family of snake venom proteins veficolins from *Cerberus rynchops* using a venom gland transcriptomics and proteomics approach, J. Proteome Res. 9 (2010) 1882–1893.
[12] C.L. Weldon, S.P. Mackessy, Biological and proteomic analysis of venom from the Puerto Rican Racer (*Alsophis Portoricensis*: Dipsadidae), Toxicon 55 (2010) 558–569.
[13] D. Georgieva, J. Seifert, M. Ohler, M. Von Bergen, P. Spencer, R.K. Arni, N. Genov, C. Betzel, *Pseudechis australis* venomics: adaptation for a defense against microbial pathogens and recruitment of body transferrin, J. Proteome Res. 10 (2011) 2440–2464.
[14] K. Kulkeaw, W. Chaicumpa, Y. Sakolvaree, P. Tongtawe, P. Tapchaisri, Proteome and immunome of the venom of the thai cobra, *Naja kaouthia*, Toxicon 49 (2007) 1026–1041.
[15] D. Petras, L. Sanz, A. Segura, M. Herrera, M. Villalta, D. Solano, M. Vargas, G. Leon, D.A. Warrell, R.D. Theakston, R.A. Harrison, N. Durfa, A. Nasidi, J.M. Gutierrez, J.J. Calvete, Snake venomics of African spitting cobras: toxin composition and assessment of congeneric cross-reactivity of the pan-African EchiTAb-Plus-ICP antivenom by antivenomics and neutralization approaches, J. Proteome Res. 10 (2011) 1266–1280.
[16] L. St Pierre, G.W. Birrell, S.T. Earl, T.P. Wallis, J.J. Gorman, J. De Jersey, P.P. Masci, M.F. Lavin, Diversity of toxic components from the venom of the evolutionarily distinct black whip snake, *Demansia vestigiata*, J. Proteome Res. 6 (2007) 3093–3107.
[17] L. Quinton, J.P. Le Caer, G. Phan, C. Ligny-Lemaire, J. Bourdais-Jomaron, F. Ducancel, J. Chamot-Rooke, Characterization of toxins within crude venoms by combined use of fourier transform mass spectrometry and cloning, Anal. Chem. 77 (2005) 6630–6639.
[18] J.W. Fox, S.M. Serrano, Insights into and speculations about snake venom metalloproteinase (SVMP). Synthesis, folding and disulfide bond formation and their contribution to venom complexity, FEBS J. 275 (2008) 3016–3030.
[19] J.W. Fox, S.M. Serrano, Timeline of key events in snake venom metalloproteinase research, J. Proteomics 72 (2009) 200–209.
[20] D.H. Souza, M.R. Iemma, L.L. Ferreira, J.P. Faria, M.L. Oliva, R.B. Zingali, S. Niewiarowski, H.S. Selistre-de-Araujo, The disintegrin-like domain of the snake venom metalloprotease alternagin inhibits alpha2beta1 integrin-mediated cell adhesion, Arch. Biochem. Biophys. 384 (2000) 341–350.
[21] M.R. Cominetti, C.H. Terruggi, O.H. Ramos, J.W. Fox, A. Mariano-Oliveira, M.S. De Freitas, C.C. Figueiredo, V. Morandi, H.S. Selistre-de-Araujo, Alternagin-C, a disintegrin-like protein, induces vascular endothelial cell growth factor (VEGF) expression and endothelial cell proliferation in vitro, J. Biol. Chem. 279 (2004) 18247–18255.
[22] P. Zigrino, A.S. Kamiguti, J. Eble, C. Drescher, R. Nischt, J.W. Fox, C. Mauch, The reprolysin jararhagin, a snake venom metalloproteinase, functions as a fibrillar collagen agonist involved in fibroblast cell adhesion and signaling, J. Biol. Chem. 227 (2002) 40528–40535.
[23] J.M. Gutiérrez, A. Rucavado, T. Escalante, C. Díaz, Hemorrhage induced by snake venom metalloproteinases: biochemical and biophysical mechanisms involved in microvessel damage, Toxicon 45 (2005) 997–1011.
[24] F.S. Markland Jr., S. Swenson, Snake venom metalloproteinases, Toxicon 62 (2013) 3–18.
[25] J.M. Gutiérrez, A. Rucavado, Snake venom metalloproteinases: their role in the pathogenesis of local tissue damage, Biochemie 82 (2000) 841–850.
[26] J.D. Phillipson, L.A. Anderson, Ethnopharmacology and western medicine, J. Ethnopharmacol. 25 (1989) 61–72.
[27] W. Martz, Plants with a reputation against snakebite, Toxicon 30 (1992) 1131–1142.
[28] W.B. Mors, M.C. Nascimento, B.M.R. Pereira, N.A. Pereira, Plant natural products active against snake bite – the molecular approach, Phytochem 55 (2000) 627–642.
[29] A.M. Soares, A.H. Januário, M.V. Lourenço, A.M.S. Pereira, P.S. Pereira, Neutralizing effects of snake venoms exhibited by Brazilian plants, Drugs Future 29 (2004) 1105–1117.
[30] A.M. Soares, F.K. Ticli, S. Marcussi, M.V. Lourenço, A.H. Januário, S.V. Sampaio, B. Lomonte, P.S. Pereira, Medicinal plants with inhibitory properties against snake venoms, Curr. Med. Chem. 12 (2005) 2625–2641.
[31] B.S. Vishwanath, T.V. Gowda, Interaction of aristolochic acid with *Vipera russelli* phospholipase A_2: its effect on enzymatic and pharmacological activities, Toxicon 25 (1987) 929–937.
[32] S. Marcussi, C.D. SantAna, C.Z. Oliveira, A.Q. Rueda, D.L. Menaldo, R. Beleboni, R.G. Stábeli, J.R. Giglio, M.R.M. Fontes, A.M. Soares, Snake venom phospholipase A_2 inhibitors: medicinal chemistry and therapeutic potential, Curr. Top. Med. Chem. 7 (2007) 743–756.
[33] M.F. Batina, A.C. Cintra, E.L. Veronese, M.A. Lavrador, J.R. Giglio, P.S. Pereira, D.A. Dias, S.C. França, S.V. Sampaio, Inhibition of the lethal and myotoxic activities of *Crotalus durissus terrificus* venom by *Tabernaemontana catharinensis*: identification of one of the active components, Planta Med. 66 (2000) 424–428.
[34] Q.B. Li, R. Pan, G.F. Wang, S.X. Tang, Anisodamine as an effective drug to treat snakebites, J. Nat. Toxins 8 (1999) 327–330.
[35] K.S. Girish, K. Kemparaju, Inhibition of *Naja naja* venom hyaluronidase by plant-derived bioactive components and polysaccharides, Biochem. Mosc. 70 (2005) 948–952.
[36] G. Viola, L. Facciolo, S. Dall'Acqua, F. Di Lisa, M. Canton, D. Vedaldi, A. Fravolini, O. Tabarrini, V. Cechetti, 6-Aminoquinolones: photostability, cellular distribution and phototoxicity, Toxicol. vitro 18 (2004) 581–592.
[37] J.P. Michael, Quinoline, quinazoline and acridone alkaloids, Nat. Prod. Rep. 21 (2004) 650–668.
[38] G. Anquetin, J. Greiner, P. Vierling, Quinolone-based drugs against *Toxoplasma gondii* and *Plasmodium spp*, Curr. Drug Targets Infect. Disord. 5 (2005) 227–245.
[39] S. Marcussi, C.P. Bernardes, N.A. Santos-Filho, M.V. Mazzi, C.Z. Oliveira, L.F.M. Izidoro, A.L. Fuly, A.J. Magro, A.S.K. Braz, M.R.M. Fontes, J.R. Giglio, A.M. Soares, Molecular and functional characterization of a new non-hemorrhagic metalloprotease from *Bothrops jararacussu* snake venom with antiplatelet activity, Peptides 28 (2007) 2328–2339.
[40] M.V. Mazzi, S. Marcussi, G.B. Carlos, R.G. Stabeli, J.J. Franco, F.K. Ticli, A.C.O. Cintra, S.C. França, A.M. Soares, S.V. Sampaio, A new hemorrhagic (fibrinogenolytic) metalloprotease from *Bothrops jararacussu* snake venom: isolation and biochemical characterization, Toxicon 44 (2004) 215–223.
[41] V.M. Rodrigues, A.M. Soares, R. Guerra-Sá, V. Rodrigues, M.R.M. Fontes, J.R. Giglio, Structural and functional characterization of neuwiedase, a non-hemorrhagic fibrin(ogen)olytic metalloprotease from *Bothrops neuwiedi* snake venom, Arch. Biochem. Biophys. 381 (2000) 213–224.
[42] J. Söding, A. Biegert, A.N. Lupas, The HHpred interactive server for protein homology detection and structure prediction, Nucl. Acids Res. 33 (2005) 244–248.
[43] T.J. Lingott, C. Schleberger, J.M. Gutiérrez, I. Merfort, High-resolution crystal structure of the snake venom metalloproteinase BaP1 complexed with a peptidomimetic: insight into Inhibitor binding, Biochemistry 48 (2009) 6166–6174.
[44] M.A. Marti-Renom, A. Stuart, A. Fiser, R. Sanchez, F. Melo, A. Sali, Comparative protein structure modeling of genes and genomes, Annu. Rev. Biophys. Biomol. Struct. 29 (2000) 291–325.
[45] L. Watanabe, J.D. Shannon, R.H. Valente, A. Rucavado, A. Alape-Giron, A.S. Kamiguti, R.D. Theakston, J.W. Fox, J.M. Gutiérrez, R.K. Arni, Amino acid sequence and crystal structure of BaP1, a metalloproteinase from *Bothrops asper* snake venom that exerts multiple tissue-damaging activities, Protein Sci. 12 (2003) 2273–2281.
[46] S.C. Lovell, I.W. Davis, W.B. Arendall III, P.I.W. de Bakker, J.M. Word, M.G. Prisant, J.S. Richardson, D.C. Richardson, Structure validation by Calpha geometry: phi, psi and Cbeta deviation, Proteins Struct. Funct. Genet. 50 (2003) 437–450.
[47] M. Wiederstein, M.J. Sippl, ProSA-web: interactive web service for the recognition of errors in three-dimensional structures of proteins, Nucleic Acids Res. 35 (2007) W407–W410.
[48] M.D. Hanwell, D.E. Curtis, D.C. Lonie, T. Vandermeersch, E. Zurek, G.R. Hutchison, Avogadro: an advanced semantic chemical editor, visualization, and analysis platform, J. Cheminform. 4 (2012) 17.
[49] G. Jones, P. Willett, R.C. Glen, Molecular recognition of receptor sites using a genetic algorithm with a description of desolvation, J. Mol. Biol. 245 (1995) 43–53.
[50] H.J.C. Berendsen, D. van der Spoel, R. Van Drunen, GROMACS: a message-passing parallel molecular dynamics implementation, Comp. Phys. Commun. 91 (1995) 43–56.
[51] B. Hess, C. Kutzner, D. van der Spoel, E. Lindahl, GROMACS 4: algorithms for highly efficient, load-balanced, and scalable molecular simulation, J. Chem. Theory Comput. 4 (2008) 435–447.
[52] C. Oostenbrink, T.A. Soares, N.F.A. van der Vegt, W.F. van Gunsteren, Validation of the 53A6 GROMOS force field, Eur. Biophys. J. 34 (2005) 273–284.
[53] H.J.C. Berendsen, J.P.M. Postma, W.F. van Gunsteren, J. Hermans, Interaction models for water in relation to protein hydration, in: B. Pullman (Ed.), Intermolecular Forces, D. Reidel Publishing Co., Dordrecht, 1981, pp. 331–342.
[54] H.J.C. Berendsen, J.P.M. Postma, W.F. van Gunsteren, A. DiNola, J.R. Haak, Molecular dynamics with coupling to an external bath, J. Chem. Phys. 81 (1984) 7.
[55] C. Andreini, L. Banci, I. Bertini, S. Elmi, A. Rosato, Comparative analysis of the ADAM and ADAMTS families, J. Protein Res. 4 (2005) 881–888.
[56] D. Edmont, R. Rocher, C. Plisson, J. Chenault, Synthesis and evaluation of quinoline carboxyguanidines as antidiabetic agents, Bioorg. Med. Chem. Lett. 10 (2000) 1831–1834.
[57] F.X. Gomis-Rüth, L.F. Kress, W. Bode, First structure of a snake venom metalloproteinase: a prototype for matrix metalloproteinases/collagenases, EMBO J. 12 (1993) 4151–4157.
[58] F.X. Gomis-Rüth, E.F. Meyer, L.F. Kress, V. Politi, Structures of adamalysin II with peptidic inhibitors. Implications for the design of tumor necrosis factor α convertase inhibitors, Protein Sci. 7 (1998) 283–292.
[59] D. Zhang, I. Botos, F.X. Gomis-Rüth, R. Doll, C. Blood, F.G. Njoroge, J.W. Fox, W. Bode, E.F. Meyer, Structural interaction of natural and synthetic inhibitors with the venom metalloproteinase, atrolysin C (form d), Proc. Natl. Acad. Sci. U. S. A. 91 (1994) 8447–8451.
[60] T. Kumasaka, M. Yamamoto, H. Moriyama, N. Tanaka, M. Sato, Y. Katsube, Y. Yamakawa, T. Omori-Satoh, S. Iwanaga, T. Ueki, Crystal structure of H2-proteinase from the venom of *Trimeresurus flavoviridis*, J. Biochem. 119 (1996) 49–57.
[61] W. Gong, X. Zhu, S. Liu, M. Teng, L. Niu, Crystal structures of acutolysin A, a three-disulfide hemorrhagic zinc metalloproteinase from the snake venom of *Agkistrodon acutus*, J. Mol. Biol. 283 (1998) 657–668.
[62] X. Zhu, M. Teng, L. Niu, Structure of acutolysin-C, a haemorrhagic toxin from

the venom of *Agkistrodon acutus*, providing further evidence for the mechanism of the pH-dependent proteolytic reaction of zinc metalloproteinases, Acta Cryst. D55 (1999) 1834–1841.
[63] K.F. Huang, S.H. Chiou, T.P. Ko, A.H. Wang, Determinants of the ihibition of a Taiwan habu venom metalloproteinase by its endogenous inhibitors revealed by X-ray crystallography and synthetic inhibitor analogues, Eur. J. Biochem. 269 (2002) 3047–3056.
[64] J.R.C. Muniz, A.L.B. Ambrósio, H.S. Selistre-de-Araújo, M.R. Cominetti, A.M. Moura-da-Silva, G. Oliva, R.C. Garratt, D.H.F. Souza, The three-dimensional structure of Bothropasin, the main hemorrhagic factor from *Bothrops jararaca* venom: insights for a new classification of snake venom metalloprotease subgroups, Toxicon 52 (2008) 807–816.
[65] M. Cirilli, C. Gallina, E. Gavuzzo, C. Giordano, F.X. Gomis-Rüth, B. Gorini, L.F. Kress, F. Mazza, M.P. Paradisi, G. Pochetti, V. Politi, 2 Å x-Ray structure of adamalysin II complexed with a peptide phosphonate inhibitor adopting a retro-binding mode, FEBS Lett. 418 (1997) 319–322.
[66] W. Stöcker, F. Grams, U. Baumann, P. Reinemer, F.X. Gomis-Rüth, D.B. McKay, W. Bode, The metzincins – topological and sequential relations between the astacins, adamalysins, serralysins, and matrixins (collagenases) define a superfamily of zinc-peptidases, Protein Sci. 4 (1995) 823–840.
[67] C. Andreini, G. Cavallaro, S. Lorenzini, FindGeo: a tool for determining metal coordination geometry, Bioinformatics 28 (2012) 1658–1660.